American Mineralogist, Volume 80, pages 213–221, 1995

Magnetic properties of the magnetite-spinel solid solution: Saturation magnetization and cation distributions

RICHARD J. HARRISON, ANDREW PUTNIS
Department of Earth Sciences, University of Cambridge, Downing Street, Cambridge CB2 3EQ, U.K.

ABSTRACT

Magnetic hysteresis properties of the Fe_3O_4-$MgAl_2O_4$ solid solution have been measured at 4.4 K and in fields up to 12 T. The trend in saturation magnetization, M_s (4.4 K), as a function of composition is consistent with the cation distribution model of Nell and Wood (1989) and suggests that M_s (4.4 K) changes sign at a composition of 30 mol% Fe_3O_4. The change in sign of M_s (4.4 K) at this composition is correlated with an anomalous peak in coercivity of over 700 mT. This effect has been explained in terms of fluctuations in both composition and the degree of nonconvergent cation order, which lead to fine-scale magnetic domains with antiferromagnetic exchange coupling.

INTRODUCTION

Magnetic minerals exist with a wide range of microstructures associated with oxidation, subsolidus exsolution, or cation ordering (Haggerty, 1991). In magnetic spinel solid solutions, the processes of nonconvergent cation ordering and phase separation occur concurrently, both of which lead to heterogeneities in composition, cation distribution, and strain. Microstructures associated with these heterogeneities occur almost universally in samples and may be responsible for the unusually high coercivities observed in coarse-grained material (Tucker and O'Reilly, 1980; Shive and Butler, 1969; Price, 1980; Evans and Wayman, 1974). Microstructures associated with convergent cation ordering in the system hematite-ilmenite have been shown to interact strongly with magnetic properties, leading to domain-wall pinning and self-reversed thermoremanent magnetization (Nord and Lawson, 1989, 1992; Brown et al., 1993; Hoffman, 1992; Varea and Robledo, 1987). An understanding of the magnetic properties of heterogeneous systems is therefore fundamental to the interpretation of remanent magnetizations and their stability over geological time.

Studying the development of heterogeneous spinels and the consequences for magnetic properties requires a spinel solid solution with a high-temperature miscibility gap so that exsolution may be induced on a laboratory time scale. Although magnetism in titanomagnetites is the most important cause of remanence in natural rocks, such experiments are not possible with the titanomagnetite solid solution because of the low temperatures required for spinodal decomposition (Price, 1981). The solid solution between magnetite (Fe_3O_4) and spinel ($MgAl_2O_4$) is a more suitable system in that it consists of magnetic and nonmagnetic end-members, there is a large variation in Curie temperature across the solid solution (Nishitani, 1981), the chemical solvus has a consolute point near 1000 °C (Mattioli and Wood, 1988), and there are extensive changes in the degree of nonconvergent cation ordering as a function of temperature (Nell and Wood, 1989; Nell et al., 1989). Previous experimental work on this binary includes measurements of lattice parameters, magnetite activity, Curie temperature, room-temperature low-field magnetization, and cation distribution vs. composition (Mattioli et al., 1987; Mattioli and Wood, 1988; Nishitani, 1981; Nell et al., 1989).

The magnetic properties of a ferrimagnetic solid solution are dependent on the cation distribution (Stephenson, 1969, 1972a, 1972b; Readman and O'Reilly, 1972). In the case of spinel solid solutions, general formula AB_2O_4, the important factor is the distribution of paramagnetic ions between tetrahedral (A) sites and octahedral (B) sites, the net magnetization of the spinel being the difference between the A and B sublattice magnetizations (Brown et al., 1993). In complex Fe-Mg-Al spinels, a complete experimental determination of the cation distribution is made difficult by the existence of four cations on both octahedral and tetrahedral sites. The distributions of Fe^{2+} and Fe^{3+} ions between sites may be determined by combinations of thermopower, conductivity, and Mössbauer techniques (Nell et al., 1989; Trestman-Matts et al., 1983; Schmidbauer, 1987). For the Fe_3O_4-$MgAl_2O_4$ binary, a theoretical determination of the Al distribution is required, in addition to thermopower and conductivity measurements, to determine the cation distribution completely (Nell et al., 1989). Measurements of saturation magnetization, however, provide a sensitive indication of trends or changes in cation distribution and may therefore be used as experimental tests for models of cation distributions or oxidation mechanisms (Akimoto, 1954; Readman and O'Reilly, 1972). As a preliminary to a complete study of microstructural development and magnetic properties, this work presents the results of low-temperature, high-field magnetic hysteresis measurements on synthetic samples of the magnetite-spinel solid solution, quenched from above the solvus.

0003–004X/95/0304–0213$02.00

Experimental and analytical procedures

Synthesis

The starting materials for all syntheses were 99.9% pure Fe_2O_3 and MgO (Aldrich Chemicals) and Al_2O_3 prepared by firing $AlCl_3 \cdot 6H_2O$ for 2 h at 400 °C, 5 h at 700 °C, and 1 h at 900 °C. MgO and Al_2O_3 were stored in a muffle furnace at 400 °C to prevent hydration and cooled in a desiccator prior to weighing. MgO and Al_2O_3 were weighed out in equimolar proportion and varying amounts of Fe_2O_3 added to yield compositions at approximately 10 mol% intervals along the binary. Oxides were ground together under absolute alcohol for 20 min with an agate mortar and pestle and then pressed into a pellet.

Pellets were wrapped in Pt foil, suspended in a Pt bucket, and fired at 1400 °C and log $f_{O_2} = -4.2$ for periods between 3 and 5 d in a vertical-tube gas-mixing furnace (Nafziger et al., 1971). The value of $f_{O_2} = -4.2$ was chosen to yield stoichiometry in the magnetite component of the solid solution (Deickmann, 1982). Oxygen fugacity was controlled by the ratio mixing of CO_2 and H_2 gasses using Tylan General FC-260 gas flow controllers, factory-calibrated to 4% accuracy for CO_2 and H_2. Oxygen fugacity was monitored with an yttria-stabilized zirconia solid electrolyte O_2 probe (Sato, 1971). The accuracy of the probe was checked between 1000 and 1300 °C with reference to the wüstite + magnetite buffer (Myers and Eugster, 1983) and found to be accurate to within 0.4 log unit. Measured values of the f_{O_2} during synthesis were in agreement to within 0.4 log unit of tabulated values (Deines et al., 1974).

Samples were quenched from 1400 °C by dropping directly from the furnace into water. The quench time is estimated to be $\ll 1$ s. Samples SP3, SP5, SP10, and SP12 were reground, re-pressed, and fired for an additional period at 1400 °C. Only a few samples were reground in this way so that systematic differences between samples having undergone one or two synthesis steps could be determined.

X-ray diffraction

X-ray diffractometer traces of the synthesized material were recorded using Cu$K\alpha$ radiation and a scan rate of 0.5° 2θ/min. Results suggest single-phase homogeneous spinels (based on peak sharpness and splitting of $K\alpha_1$-$K\alpha_2$ peaks), with no unreacted oxides being detected by this method. Lattice parameters were measured from X-ray powder diffraction patterns from a Guinier camera. An internal Si standard was used to correct for film shrinkage. Peak positions were measured with a vernier scale to an accuracy of $\pm 0.01°$ 2θ. Lattice parameters were then determined using around nine reflections in a least-squares procedure.

Detailed peak profiles of the 311 and 440 reflections were recorded using a Seifert automated step-scan diffractometer, with a step width of 0.01° 2θ and a counting time of 2 min per step (Cu$K\alpha$ radiation). Background intensity was modeled with a straight-line fit by least squares. The 311 profile was fitted with the sum of two Gaussian functions. The 440 profile was fitted with the sum of three Gaussian functions to take account of the $K\alpha_1$ and $K\alpha_2$ peaks.

Electron microprobe analysis

Samples were mounted in epoxy resin and polished using a minimum of 0.25 μm of SiC. The general polish quality was poor, although regions with a diameter >10 μm were good enough to probe without encountering porosity. Energy-dispersive analysis was performed using a beam current of 15 nA and a beam diameter of approximately 2 μm. Analyzed elements were Mg, Fe, and Al, using standards MgO, pure Fe metal, and Al_2O_3, respectively. O was calculated by difference and the final analyses were normalized to a formula unit containing four O atoms and three cations. This procedure yields compositions in good agreement with the expected values.

Scanning electron microscopy

Sintered chunks and crushed grains were mounted and Au coated for examination using secondary electron imaging. Estimates of the grain size using this method indicate that the majority of grains are in the range 0.5–2 μm with fewer grains with a diameter of up to 10 μm. Polished sections were C coated and examined using backscattered electron imaging to check sample homogeneity. A second phase of a Si-rich material was detected in samples SP3 and SP5. This second phase comprises around 5–10% of the sample surface and fills the spaces between polished spinel regions. Two possible sources of Si in the sample preparation are polishing with SiC or grinding with an agate mortar and pestle. If the second phase is a polishing artifact, then it does not affect the results. If it is derived during regrinding, then its presence throughout the sample may affect calculated values of the saturation magnetization. There is no systematic variation in the results to suggest this is the case, however. For example, M_s (4.4 K) for samples SP11 ($x = 0.508$, ground once) and SP12 ($x = 0.51$, ground twice) differ by only 0.05 μ_b per formula unit.

Results of sample characterization

Electron microprobe analyses of the synthetic samples are presented in Table 1. The composition of the samples with respect to the Fe_3O_4-$MgAl_2O_4$ binary is illustrated in Figure 1. Approximate compositions of the samples are defined in terms of the ideal solid solution $(Fe_3O_4)_x(MgAl_2O_4)_{1-x}$, where x is calculated from the analysis by dividing the analyzed Fe content per formula unit by three. The standard deviation in x is typically <0.01 for the 20 analyses, and the samples do not appear to be zoned. The single-phase nature of the samples has been confirmed by TEM investigation. Figure 2 shows the variation in lattice parameter vs. composition. There is good agreement with previous results for the stoichiometric solid solution (Mattioli et al., 1987).

Peak profiles of the 311 and 440 reflections in sample

TABLE 1. Electron microprobe analyses of synthetic spinels

Sample	MgO (wt%)	Al_2O_3 (wt%)	FeO (wt%)	Total (wt%)	Mg*	Al*	Fe*	x*	Al/Mg
SP2	24.98(0.67)	60.72(1.23)	13.24(0.58)	98.95(1.65)	0.93(0.01)	1.79(0.01)	0.28(0.01)	0.092(0.005)	1.92(0.03)
SP3	21.29(0.21)	55.43(0.57)	22.98(0.19)	99.70(0.73)	0.82(0.004)	1.69(0.005)	0.50(0.006)	0.165(0.002)	2.06(0.01)
SP4	28.24(0.93)	67.72(1.87)	0.012(0.02)	95.96(2.79)	1.04(0.006)	1.96(0.006)	0(0)	0(0)	1.90(0.015)
SP5	18.87(0.11)	48.52(0.23)	31.06(0.13)	98.45(0.26)	0.76(0.003)	1.54(0.005)	0.70(0.005)	0.233(0.002)	2.03(0.01)
SP6	17.25(0.17)	42.63(0.36)	37.96(0.23)	97.84(0.59)	0.72(0.004)	1.40(0.005)	0.88(0.006)	0.295(0.002)	1.95(0.013)
SP9	13.75(0.28)	33.74(0.47)	50.40(0.44)	97.90(0.77)	0.60(0.008)	1.16(0.01)	1.23(0.013)	0.412(0.004)	1.94(0.03)
SP10	15.31(0.27)	38.08(0.65)	44.75(0.32)	98.14(0.70)	0.65(0.006)	1.28(0.01)	1.07(0.02)	0.356(0.005)	1.97(0.015)
SP11	10.84(0.51)	27.02(0.94)	59.13(0.95)	96.98(0.51)	0.50(0.01)	0.98(0.03)	1.52(0.03)	0.508(0.01)	1.97(0.04)
SP12	10.69(0.22)	26.78(0.39)	59.17(0.23)	96.64(0.70)	0.49(0.006)	0.98(0.007)	1.53(0.01)	0.510(0.004)	1.98(0.02)
SP13	8.10(0.32)	20.55(1.48)	67.54(1.53)	96.20(0.38)	0.39(0.01)	0.78(0.05)	1.83(0.003)	0.609(0.02)	2.00(0.09)

Note: numbers in parentheses are one standard deviation.
* Based on a formula unit with three cations per four O atoms.

SP11 are shown in Figure 3. Both reflections show significant diffuse scattering at the base of the main peak. Pure positional or compositional disorder in a solid solution produces diffuse scattering, which contributes only to the general background (Guinier, 1963). If, however, the disorder consists of correlated changes in lattice spacing and structure factor (i.e., coupled compositional and positional disorder), then diffuse scattering may concentrate at the diffraction peaks. The effect may be enhanced by short-range ordering or clustering of cations prior to exsolution. Hence the observed diffuse scattering is consistent with, but does not necessarily require, the presence of heterogeneities in composition or degree of cation order.

MAGNETIC MEASUREMENTS

Magnetic hysteresis loops were measured at 4.4 K and in fields up to 12 T, with an Oxford Instruments vibrating sample magnetometer, equipped with a superconducting magnet. Sintered chunks with a mass of 0.007–0.026 g and a diameter of 3–5 mm were placed on the end of a plastic sample holder and held in place with several layers of PTFE tape. The temperature of the sample was held near 4.4 K by balancing the output from a resistive heater with a flow of He gas through the superconducting magnet bore. Temperature was measured with a thermocouple to an accuracy of ±0.1 K and varied between 4.3 and 5 K during the time taken to measure each hysteresis loop (≈50 min). Magnetization was measured as a function of applied field with a field ramp rate of 20 mT/s. The high ramp rate was necessary to complete measurements in a

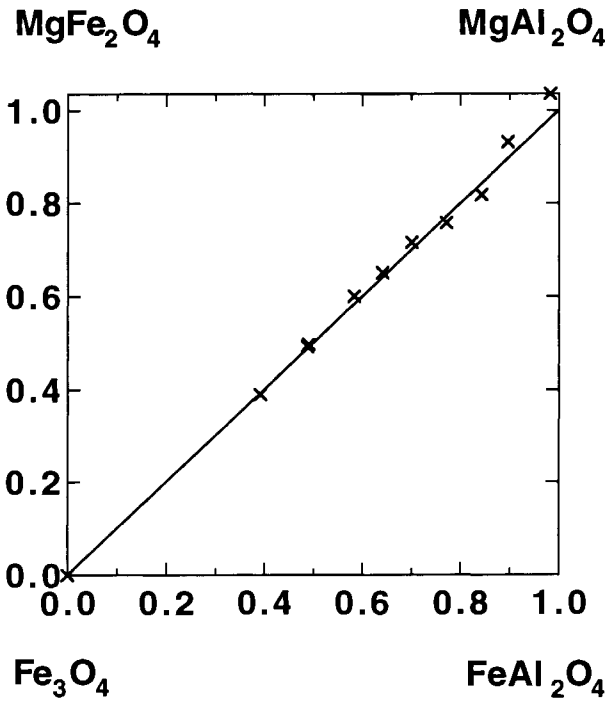

Fig. 1. Compositions of synthesized samples (Xs) in terms of the quaternary system Fe_3O_4-$FeAl_2O_4$-$MgAl_2O_4$-$MgFe_2O_4$, as determined by electron microprobe analysis. The solid line represents compositions on the ideal Fe_3O_4-$MgAl_2O_4$ binary join.

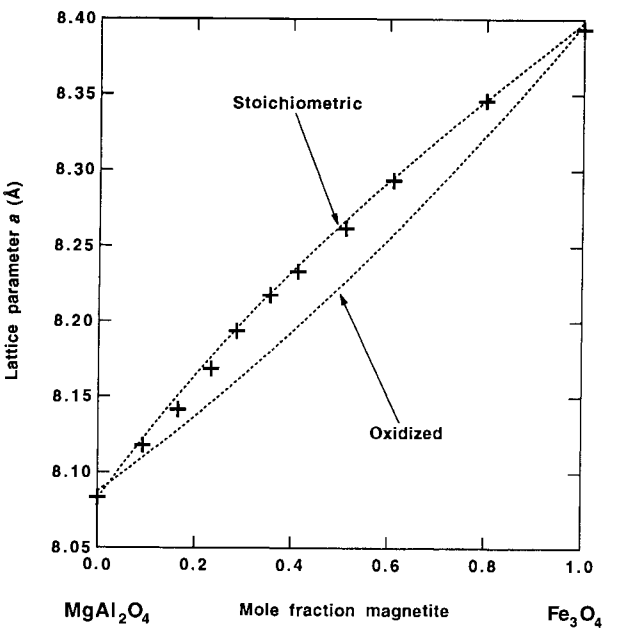

Fig. 2. Lattice parameters of synthetic samples (plus signs) as a function of magnetite content (x). Dashed lines are the results of Mattioli et al. (1987) for the stoichiometric and oxidized solid solution.

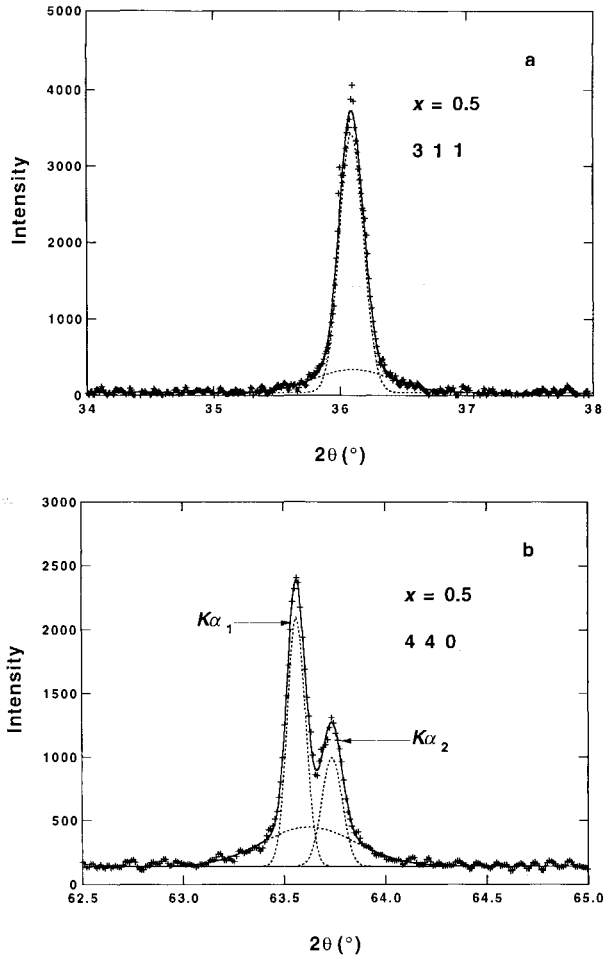

Fig. 3. Step-scan diffractometer peak profiles of the 311 (**a**) and 440 (**b**) reflections in sample SP11 ($x = 0.5$). The solid line is the resultant fit to the raw intensity data (plus signs), using the sum of two Gaussians for reflection 311 and the sum of three Gaussians for reflection 440. The individual Gaussian components are shown as dashed lines.

reasonable time. The estimated error in magnetization measurements is $<10^{-8}$ Am^2.

The value of the saturation magnetization (i.e., magnetization in an infinite applied field) was determined by fitting the high-field portion of the initial magnetization curve (from 4 to 12 T), with an equation of the form $M = M_s(1 - a/H) + kH$, where M_s is the saturation magnetization, H is the applied field, and a and k are constants (Brown et al., 1993). The kH term is due to the forced magnetization in very high fields. Excellent fits to the magnetization curves were possible.

Results of magnetic measurements

Eleven hysteresis loops for samples of various composition along the binary were measured, four of which are presented in Figure 4. There is a clear transition in the characteristic shape of the hysteresis loops toward the spinel-rich end of the solid solution. In particular, there is a large variation in the field required to reduce the magnetization to zero (i.e., the coercivity). Magnetite-rich samples have low coercivities and are fully saturated in fields >2 T. Spinel-rich samples have extremely large coercivities and do not appear to saturate, even in the maximum field of 12 T. The values of the saturation magnetization per formula unit and the coercive force are presented in Figure 5. Our confidence in the results for M_s (4.4 K) is high because of the low errors involved in the measurement of magnetization and the ideal conditions under which they were obtained. The error in the given value of the coercive force is large, however, because of the poor resolution achieved with a field ramp rate of 20 mT/s.

Table 2. Saturation magnetization, M_s (4.4 K) and coercivity, H_c, of synthetic spinels

Composition (x)	M_s (4.4 K) (μ_b)	H_c (mT)
0.09	0.35	5
0.17	0.28	39
0.23	0.27	235.7
0.3	0.26	715.6
0.36	0.36	392.4
0.41	0.39	169.9
0.51	0.84	45.8
0.51	0.89	51.1
0.61	1.27	28.3
0.8*	2.23	10
1	3.92	10

* Apparent composition.

The saturation magnetization for the pure magnetite end-member, given in Table 2, is 3.9 μ_b per formula unit ($1\ \mu_b = 9.27 \times 10^{-24}$ Am^2), compared with an ideal value of 4.1 μ_b. This may suggest some degree of nonstoichiometry in this sample (Readman and O'Reilly, 1972). M_s (4.4 K) falls to a minimum of 0.26 μ_b pfu as the composition varies between $x = 1$ and $x = 0.3$. It then rises to a maximum of 0.35 μ_b at $x = 0.09$ before falling to zero in the pure spinel end-member. The minimum in the M_s (4.4 K) curve at $x = 0.3$ is correlated with a peak coercivity of over 700 mT.

Discussion

Thermodynamics and cation distributions

The variation in saturation magnetization as a function of composition must be accounted for in terms of the distribution of Fe^{3+} and Fe^{2+} ions between octahedral and tetrahedral sites. The equilibrium cation distribution has been calculated for this solid solution as a function of temperature and composition using an existing thermodynamic model, calibrated for the Fe-Mg-Al quaternary (Nell and Wood, 1989). Calculations were performed by solving numerically the three nonlinear simultaneous equations given by Nell and Wood (1989) for the quaternary system, with compositions restricted to the Fe_3O_4-$MgAl_2O_4$ binary (see Eqs. 25–27, Nell and Wood, 1989). The expected saturation magnetization was

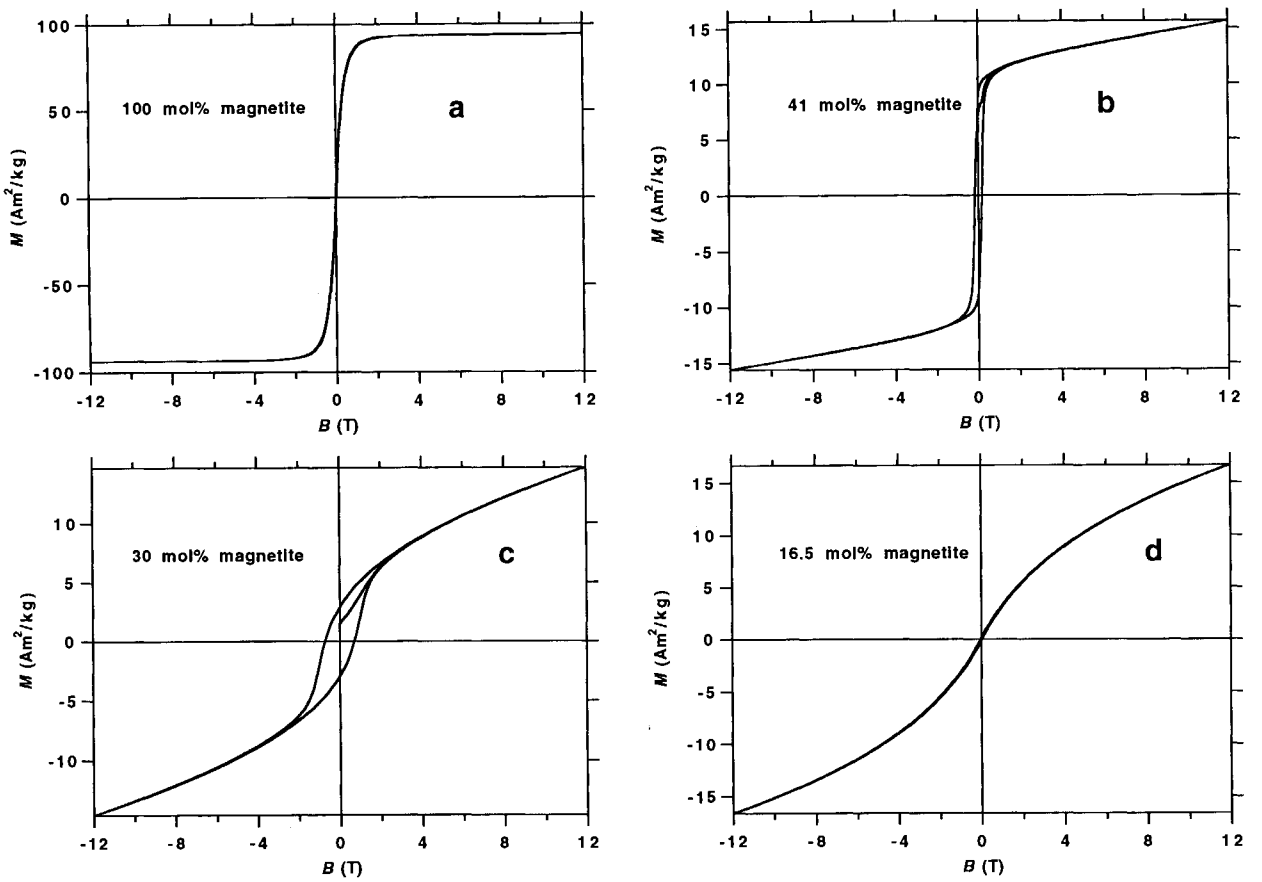

Fig. 4. Magnetization per unit mass, M (Am²/kg), vs. applied field, B (T), for samples (**a**) SP15, (**b**) SP9, (**c**) SP6, and (**d**) SP3.

then derived directly from the calculated cation distribution, assuming a spin-only moment of 4 μ_b for Fe^{2+} ions and 5 μ_b for Fe^{3+} ions. One Bohr magneton is the magnetic dipole moment associated with a single unpaired electron spin (1 $\mu_b = 9.27 \times 10^{-24}$ Am²). Results for a temperature of 1200 °C are given in Figure 6. The magnetization measured at 4.4 K is lower than that of the theoretical magnetization because of the effects of order-parameter saturation at low temperature (Salje et al., 1991). Magnetic order-parameter saturation is a quantum effect, causing $dM_s(T)/dT$ to approach zero as T approaches zero. The effect has been observed in the titanohematite system (Brown et al., 1993). The comparison between observed and calculated magnetizations in Figure 6 is hence intended only as an indicator of the trend in magnetization vs. composition.

The thermodynamic model predicts that, for magnetite-rich compositions, the solid solution is ferromagnetic with the B sublattice magnetization greater than the A sublattice magnetization (M_s is positive). At some intermediate composition, x_c, there is a compensation point where the solid solution is antiferromagnetic with the A and B sublattice magnetizations equal. For more spinel-rich compositions the solid solution becomes ferromagnetic with the A sublattice magnetization greater than the B sublattice magnetization (M_s is negative). In this context, the sign of the saturation magnetization indicates whether the net magnetization of the sample is parallel or antiparallel to the B sublattice magnetization. The magnetization experiments measure only the modulus of M_s, as indicated by the dashed line in Figure 6. The compensation point shifts toward more magnetite-rich compositions with decreasing temperature. An exact compensation point exists only for an ideal structural state, where the composition and degree of nonconvergent cation order remain homogeneous. A real crystal is heterogeneous on some scale and hence has a value of M_s that is an average over all compositional and ordering fluctuations. In this case, we would expect to see M_s fall to a minimum at x_c. Hence the experimental results presented here are consistent with the existence of a compensation point at $x_c \approx 0.3$, samples with $x < x_c$ having their net magnetization reversed with respect to those with $x > x_c$.

Coercive force at the compensation point: Speculation

The grain size of all samples is mostly in the range of 0.5–2 μm. There is no systematic variation in the average grain size across the solid solution. At room temperature

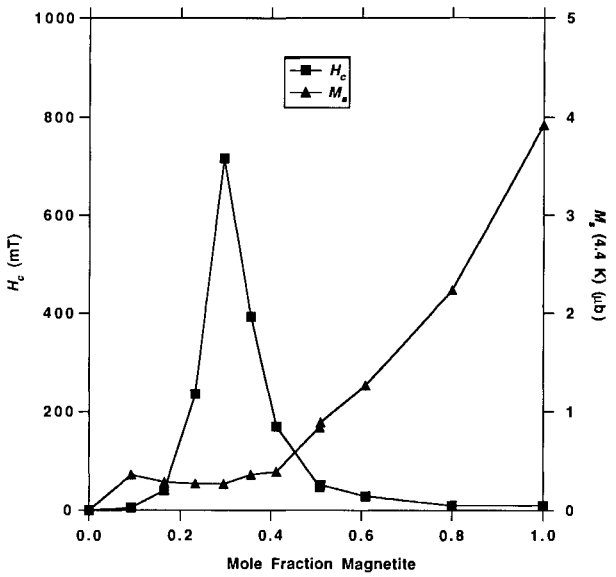

Fig. 5. Saturation magnetization per formula unit, M_s (4.4 K) (μ_b), and coercive force, H_c (mT), vs. composition. The compensation point, x_c, corresponds to the minimum in the saturation magnetization curve at $x = 0.3$ (30 mol% magnetite); 1 $\mu_b = 9.27 \times 10^{-24}$ Am^2.

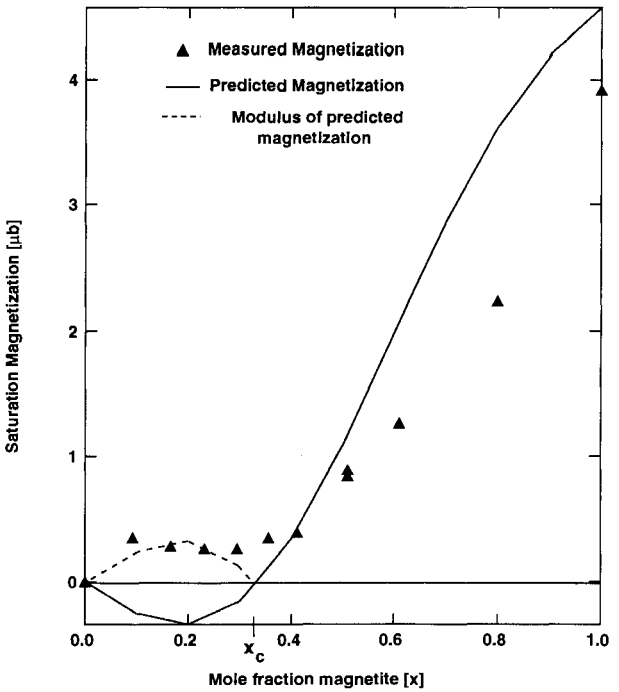

Fig. 6. Predicted variation in saturation magnetization vs. composition, using the cation distribution model of Nell and Wood (1989) and spin-only moments of 4 μ_b for Fe^{2+} and 5 μ_b for Fe^{3+}. The cation distribution is calculated in intervals of 10 mol% for a temperature of 1200 °C. The solid line is the predicted saturation magnetization. The dashed line is the modulus of predicted magnetization, i.e., the quantity measured in the hysteresis experiments. The triangles are our measured values for the saturation magnetization.

we would expect the grains to display multidomain or pseudo-single-domain properties (Dunlop, 1990). The expected magnetic domain state at 4.4 K depends on the temperature variation of anisotropy constants, exchange constants, and magnetostriction. In general, the equilibrium number of domain walls decreases with temperature, and hence it is likely that samples are either single domain or contain very few conventional magnetic domain walls.

The origin of coercivity in many magnetic materials is still a subject of much debate in the literature. Current theories on coercivity mechanisms in permanent magnet materials were reviewed by Livingston (1981) and Zijlstra (1982). In the present case, we must consider coercivity mechanisms that operate in single-phase material containing fluctuations in composition or degree of cation ordering. Such a mechanism must account for both the magnitude and compositional dependence of H_c. Typical theories deal with the pinning of conventional magnetic domain walls by strain or by fluctuations in the magnetic anisotropy and exchange constants (Jatau and Della Torre, 1993a, 1993b, 1994; Jatau et al., 1994). Such fluctuations change the energy of a domain wall locally, either pinning the wall or providing a barrier to wall motion. Calculation of the expected coercivity from such a mechanism is not possible without knowledge of the compositional dependence of anisotropy and exchange constants and information about the wavelength and amplitude of the fluctuations.

Giant intrinsic coercivities have been observed in many highly magnetic anisotropy materials at cryogenic temperatures (Oesterreicher, 1978). An example is $SmCo_{5-x}Ni_x$, which has a maximum intrinsic coercivity of 23 T at 4.2 K. This results from the fact that the widths of magnetic domain walls in highly anisotropic materials are of the same order of magnitude as the lattice spacing. For these thin walls, the energy of the wall is larger when the center of the wall coincides with an atomic plane rather than lying just either side of it (Zijlstra, 1982). This leads to a large intrinsic resistance to wall motion (analogous to the Peierls stress experienced by dislocations). The high coercivity in $SmCo_{5-x}Ni_x$ is extremely dependent on composition, with a pronounced peak in the coercivity spectrum at $x = 4$. The compositional dependence may be interpreted in terms of fluctuations in the exchange constant. A possible explanation for the large increase in coercivity at the compensation point is proposed below.

If the above model for the cation distribution is correct, then fluctuations in composition, close to x_c, will lead to adjacent domains of opposed magnetization. The same effect results from a sample of homogeneous composition but fluctuating degree of cation order, due to the shifting position of the compensation point. The chemical fluc-

tuation hence produces a fine-scale magnetic domain wall. The size of the domain wall is identical to that of the fluctuation, typically 100–200 Å. A schematic model for such a domain wall is shown in Figure 7. Lateral motion of these domain walls is impossible without cooperative cation migration. Saturating the sample hence requires overcoming the strong exchange coupling between adjacent domains. The mechanism by which this might occur involves the nucleation of reverse magnetic domains with domain-wall widths smaller than the wavelength of the fluctuation. These thin walls would be easily pinned by strain or the fluctuations in exchange and anisotropy constants, which result from heterogeneities in composition and cation order. This, together with the high number and fine scale of the domains, leads to the anomalously high coercivities observed in samples near x_c.

It is interesting to compare the magnitude of the coercive force measured here with that observed in the hematite-ilmenite system (Brown et al., 1993). This system displays exchange-dominated pinning of domain walls by transition induced domain boundaries (Nord and Lawson, 1989, 1992). Brown et al. (1993) gave values for the coercive force varying between 100 and 320 mT for the temperature range 298–77 K. By linear extrapolation of their data, we obtain a coercive force of approximately 400 mT at 0 K, in samples containing a high density of domain boundaries. In samples with low densities of domain boundaries they observe coercivities of around 20 mT. There is an excellent correlation between the magnitude of the coercive force in the titanohematite system and the magnetite-spinel system. In both cases chemical heterogeneities lead to magnetic domain walls that are pinned by strong exchange interactions. The higher coercive force observed in the magnetite-spinel system may be accounted for by the extremely fine scale of the fluctuations responsible for the effect.

Fluctuations in composition or degree of cation order are to be expected in samples quenched from 1400 °C. Significant cation reordering has been observed in spinels quenched from temperatures above 1000 °C (Wood et al., 1986; Milliard et al., 1992). Such nonequilibrium behavior may give rise to kinetic microstructures (Carpenter and Salje, 1989), whereby local regions in the crystal order at a faster rate than others, enhancing any preexisting heterogeneities. Some degree of cation clustering may also be expected on account of the high-temperature solvus.

The results presented here suggest that fine-scale heterogeneities are present in spinel solid solutions quenched from high temperatures. This suggestion has significant consequences for the thermodynamic description of such systems. In particular, the assumption that the entropy of disordering in complex spinels is purely configurational (O'Neill and Navrotsky, 1984; Sack and Ghiorso, 1991; Nell and Wood, 1989) is inappropriate. This factor may contribute to some of the quantitative differences in our observed and calculated variations in cation distribution. A free energy expansion of the Landau-Ginzburg type may be more appropriate in describing nonconvergent ordering and kinetics in heterogeneous systems (Carpenter and Salje, 1989), since this approach takes account of both nonconfigurational entropy and fluctuations in the degree of order.

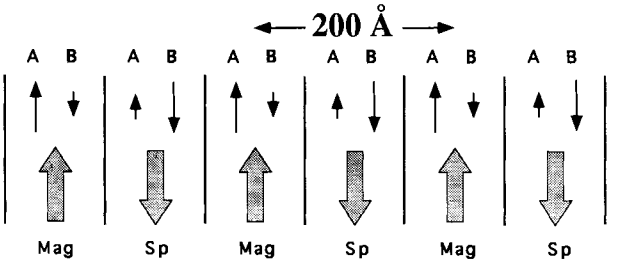

Fig. 7. Schematic model for the magnetic domain state in a sample of bulk composition $x = x_c$, containing a compositional fluctuation between magnetite-rich (Mag) and spinel-rich (Sp) regions. Solid arrows represent the magnitude and direction of tetrahedral (A) and octahedral (B) sublattice magnetizations. Shaded arrows represent the direction of net magnetization in each region of the compositional fluctuation.

Mechanism for self-reversed thermoremanent magnetization

Self-reversed thermoremanent magnetization results from the antiferromagnetic coupling between a strongly magnetic, low T_c phase and a weaker, high T_c phase (Dunlop, 1990). When cooled through the high-temperature Curie point, the weakly magnetic phase obtains a magnetization aligned parallel to the applied field. Because of the negative coupling between the two phases, the stronger magnetic phase obtains a magnetization antiparallel to that of the weaker phase when cooled through the low-temperature Curie point. Hence the net magnetization is reversed with respect to the applied field. The coupling mechanism may be either magnetostatic or exchange based (McClelland and Goss, 1993), exchange coupling being the more effective. The most common example of natural self-reversal is in the titanohematite system (Ishikawa and Syono, 1963). Self-reversal in synthetic titanohematites of composition 30% hematite and 70% ilmenite have been observed experimentally (Nord and Lawson, 1992). Here the high-T_c phase consists of Fe-enriched twin domain boundaries, which form during the $R\bar{3}c$ to $R\bar{3}$ cation ordering transition. Self-reversal in samples with compositions <50% ilmenite may be caused by exsolution of a hematite-rich phase (Carmichael, 1961; Hoffman, 1975).

A mechanism for self-reversal in homogeneous iron spinels containing significant amounts of nonmagnetic ions has been proposed previously (Verhoogen, 1956) because of changes in the equilibrium cation distribution. The mechanism operates for certain compositions when the magnetization associated with the low-temperature ordered distribution is reversed with respect to the high-temperature disordered state. A sample that is given a magnetization in the high-temperature state will obtain a

reversed magnetization after subsequent annealing at the lower temperature. This mechanism is appropriate to systems where a significant degree of cation disorder remains at the Curie temperature.

The magnetic domain structure in the Fe_3O_4-$MgAl_2O_4$ solid solution at compositions near x_c provides an ideal mechanism for self-reversed thermoremanent magnetization. There is a large variation in Curie temperature with the composition in this system. The variation of T_c with degree of cation order is unknown but is likely to be less pronounced (Moskowitz, 1987). In either case, the fluctuations in composition or cation order, which are responsible for the anomalous coercivity near x_c, produces adjacent regions with different Curie temperatures and strong negative exchange coupling. Depending on the relative amounts of magnetite-rich and spinel-rich domains, we would expect self-reversed or partial self-reversed thermoremanent magnetization to occur on cooling through the magnetic ordering temperature in an applied field. This is an important example of a self-reversing mechanism where the detailed nature of the negative exchange coupling is known, in contrast to many other proposed mechanisms, where only the presence of the second magnetic phase could be accounted for (Hoffman, 1975).

Acknowledgments

The authors would like to thank Charles Dewhurst, at the Interdisciplinary Research Centre in Superconductivity, Cambridge, for his help in making the magnetic measurements and for the use of the 12 T VSM. Many thanks to E. McClelland for her comments on an earlier version of the manuscript and to the reviewers G.L. Nord, Jr. and N.E. Brown for their useful comments and suggestions. R.J.H. acknowledges the receipt of a grant from the Natural Environment Research Council.

References cited

Akimoto, S. (1954) Thermomagnetic study of ferromagnetic minerals in igneous rocks. Journal of Geomagnetism and Geoelectricity, 6, 1–14.

Brown, N.E., Navrotsky, A., Nord, G.L., Jr., and Banerjee, S.K. (1993) Hematite-ilmenite (Fe_2O_3-$FeTiO_3$) solid solutions: Determinations of Fe-Ti order from magnetic properties. American Mineralogist, 78, 941–951.

Carmichael, C.M. (1961) The magnetic properties of ilmenite-hematite crystals. Proceedings of the Royal Society of London, 263A, 508.

Carpenter, M.A., and Salje, E. (1989) Time-dependent Landau theory for order/disorder processes in minerals. Mineralogical Magazine, 53, 483–504.

Deickmann, R. (1982) Defects and cation diffusion in magnetite: IV. Nonstoichiometry and point defect structure of magnetite ($Fe_{3-\delta}O_4$). Berichte der Bunsen Gesellschaft für Physikalische Chemie, 81, 414–419.

Deines, P., Nafziger, R.H., Ulmer, G.C., and Woermann, E. (1974) Temperature-oxygen fugacity tables for selected gas mixtures in the system C-H-O at one atmosphere total pressure. Pennsylvania State University, College of Earth and Mineral Sciences, Bulletin of the Experimental Station, 88, 129.

Dunlop, D.J. (1990) Developments in rock magnetism. Reproductions of Progress in Physics, 53, 707–792.

Evans, M.E., and Wayman, M.L. (1974) An investigation of the role of ultra-fine titanomagnetite intergrowths in paleomagnetism. Geophysics Journal of the Royal Astronomical Society, 36, 1–10.

Guinier, A. (1963) X-ray diffraction in crystals, imperfect crystals, and amorphous bodies, 378 p. Freeman, San Francisco, California.

Haggerty, S.E. (1991) Oxide textures: A mini atlas. In Mineralogical Society of America Reviews in Mineralogy, 25, 129–219.

Hoffman, K.A. (1975) Cation diffusion processes and self-reversal of thermoremanent magnetization in the ilmenite-hematite solid solution series. Geophysics Journal of the Royal Astronomical Society, 41, 65–80.

——(1992) Self-reversal of thermoremanent magnetization in the ilmenite-hematite system: Order-disorder, symmetry, and spin alignment. Journal of Geophysical Research, 97, 10883–10895.

Ishikawa, Y., and Syono, Y. (1963) Order-disorder transformation and reverse thermoremanent magnetization in the $FeTiO_3$-Fe_2O_3 system. Journal of the Physics and Chemistry of Solids, 24, 517–528.

Jatau, J.A., and Della Torre, E. (1993a) A methodology for mode pushing in coercivity calculations. IEEE Transactions on Magnetics, 29, 2374–2376.

——(1993b) One-dimensional energy barrier model for coercivity. Journal of Applied Physics, 73, 6829–6831.

——(1994) Study of the effect of defect sizes and their distribution on the coercivity of magnetic media. Journal of Applied Physics, 75, 6846–6848.

Jatau, J.A., Pardavi-Horváth, M., and Della Torre, E. (1994) Enhanced coercivity due to a local anisotropy increase. Journal of Applied Physics, 75, 6106–6108.

Livingston, J.D. (1981) Microstructure and coercivity of permanent-magnet materials. Progress in Materials Science, 41a, 243–267.

Mattioli, G.S., and Wood, B.J. (1988) Magnetite activities across the $MgAl_2O_4$-Fe_3O_4 spinel join with application to thermobarometric estimates of upper mantle oxygen fugacity. Contributions to Mineralogy and Petrology, 98, 148–162.

Mattioli, G.S., Wood, B.J., and Carmichael, I.S.E. (1987) Ternary-spinel volumes in the system $MgAl_2O_4$-Fe_3O_4-$\gamma Fe_{8/3}O_4$: Implications for the effect of P on intrinsic f_{O_2} measurements of mantle-xenolith spinels. American Mineralogist, 72, 468–480.

McClelland, E., and Goss, C. (1993) Self reversal of chemical remanent magnetization on the transformation of maghemite to hematite. Geophysics Journal International, 112, 517–532.

Milliard, R.L., Peterson, R.C., and Hunter, B.K. (1992) Temperature dependence of cation disorder in $MgAl_2O_4$ spinel using ^{27}Al and ^{17}O magic-angle spinning NMR. American Mineralogist, 77, 44–52.

Moskowitz, B.M. (1987) Towards resolving the inconsistencies in characteristic physical properties of synthetic titanomaghemites. Physics of the Earth and Planetary Interiors, 46, 173–183.

Myers, J., and Eugster, H.P. (1983) The system Fe-Si-O: Oxygen buffer calibrations to 1500K. Contributions to Mineralogy and Petrology, 82, 75–90.

Nafziger, R.H., Ulmer, G.C., and Woermann, E. (1971) Gaseous buffering for the control of oxygen fugacity at one atmosphere pressure. In G.C. Ulmer, Ed., Research techniques for high pressure and high temperature, p. 9–42. Springer-Verlag, New York.

Nell, J., and Wood, B.J. (1989) Thermodynamic properties in a multicomponent solid solution involving cation disorder: Fe_3O_4-$MgFe_2O_4$-$FeAl_2O_4$-$MgAl_2O_4$ spinels. American Mineralogist, 74, 1000–1015.

Nell, J., Wood, B.J., and Mason, T.O. (1989) High-temperature cation distributions in Fe_3O_4-$MgAl_2O_4$-$MgFe_2O_4$-$FeAl_2O_4$ spinels from thermopower and conductivity measurements. American Mineralogist, 74, 339–351.

Nishitani, T. (1981) Magnetic properties of titanomagnetites containing spinel ($MgAl_2O_4$). Journal of Geomagnetism and Geoelectricity, 33, 171–179.

Nord, G.L., Jr., and Lawson, C.A. (1989) Order-disorder transition–induced twin domains and magnetic properties in ilmenite-hematite. American Mineralogist, 74, 160–176.

——(1992) Magnetic properties of ilmenite70-hematite30: Effect of transformation-induced twin boundaries. Journal of Geophysical Research, 97B, 10897.

Oesterreicher, H. (1978) Giant intrinsic magnetic hardness. Applied Physics, 15, 341–354.

O'Neill, H.St.C., and Navrotsky, A. (1984) Cation distributions and thermodynamic properties of binary spinel solid solutions. American Mineralogist, 69, 733–753.

Price, G.D. (1980) Exsolution microstructures in titanomagnetites and their magnetic significance. Physics of the Earth and Planetary Interiors, 23, 2–12.

——— (1981) Subsolidus phase relations in the titanomagnetite solid solution series. American Mineralogist, 66, 751–758.

Readman, P.W., and O'Reilly, W. (1972) Magnetic properties of oxidized (cation deficient) titanomagnetites $(Fe,Ti,[])_3O_4$. Journal of Geomagnetism and Geoelectricity, 24, 69–90.

Sack, R.O., and Ghiorso, M.S. (1991) An internally consistent model for the thermodynamic properties of Fe-Mg-titanomagnetite-aluminate spinels. Contributions to Mineralogy and Petrology, 106, 474–505.

Salje, E.K.H., Wruck, B., and Thomas, H. (1991) Order-parameter saturation and low-temperature extension of Landau theory. Zeitschrift für Physik B–Condensed Matter, 82, 399–404.

Sato, M. (1971) Electrochemical measurements and control of oxygen fugacity with solid electrolyte systems. In G.C. Ulmer, Ed., Research techniques for high pressure and high temperature, p. 43–100. Springer-Verlag, New York.

Schmidbauer, E. (1987) Fe-57 Mössbauer spectroscopy and magnetization of cation deficient Fe_2TiO_4 and $FeCr_2O_4$: II. Magnetization data. Physics and Chemistry of Minerals, 15, 201–207.

Shive, P.N., and Butler, R.F. (1969) Stresses and magnetostrictive effects of lamellae in the titanomagnetite and ilmenohematite series. Journal of Geomagnetism and Geoelectricity, 21, 781–796.

Stephenson, A. (1969) The temperature dependent cation distribution in titanomagnetites. Geophysics Journal of the Royal Astronomical Society, 18, 199–210.

——— (1972a) Spontaneous magnetization curves and curie points of cation deficient titanomagnetites. Geophysics Journal of the Royal Astronomical Society, 29, 91–107.

——— (1972b) Spontaneous magnetization curves and curie points of spinels containing two types of magnetic ion. Philosophical Magazine, 25, 1213–1232.

Trestman-Matts, A., Doris, S.E., and Mason, T.O. (1983) Thermoelectric determination of cation distribution in Fe_3O_4-$MgFe_2O_4$. Journal of the American Ceramic Society, 67, 69–74.

Tucker, P., and O'Reilly, W. (1980) The laboratory simulation of deuteric oxidation of titanomagnetites: Effect on magnetic properties and stability of thermoremanence. Physics of the Earth and Planetary Interiors, 23, 112–133.

Varea, C., and Robledo, A. (1987) Critical magnetization at antiphase boundaries of magnetic binary alloys. Physical Review B, 36, 5561–5566.

Verhoogen, J. (1956) Ionic ordering and self-reversal of magnetization in impure magnetites. Journal of Geophysical Research, 61, 201–209.

Wood, B.J., Kirkpatrick, R.J., and Montez, B. (1986) Order-disorder phenomena in $MgAl_2O_4$ spinel. American Mineralogist, 71, 999–1006.

Zijlstra, H. (1982) Permanent magnets: Theory. In E.P. Wohlfarth, Ed., Ferro-magnetic materials: A handbook of the properties of magnetically ordered substances, p. 37–105. North-Holland, Amsterdam.

Manuscript received June 24, 1994
Manuscript accepted November 21, 1994